Enhanced structure/function of mTSPO translocator in lipid:surfactant mixed micelles

Christelle Saade, Alexandre Pozza, Françoise Bonneté, Stéphanie Finet, Viviane Lutz-Bueno, Mark Tully, Paloma Varela, Jean-Jacques Lacapère, Sophie Combet

Enhanced structure/function of mTSPO translocator in lipid:surfactant mixed micelles

Christelle SAADE[a], Alexandre POZZA[b], Françoise BONNETE[b], Stéphanie FINET[c], Viviane LUTZ-BUENO[a,d], Mark D. TULLY[e], Paloma F. VARELA[f], Jean-Jacques LACAPERE[g], and Sophie COMBET[a]*

[a]Laboratoire Léon-Brillouin (LLB), UMR12 CEA-CNRS, Université Paris-Saclay, F-91191 Gif-sur-Yvette CEDEX, France.

[b]Université Paris Cité, CNRS UMR7099, Biochimie des Protéines Membranaires, F-75005 Paris, France.

[c]Institut de Minéralogie, de Physique des Matériaux et de Cosmochimie (IMPMC), UMR 7590 CNRS-Sorbonne Université Université, MNHN, IRD, F-75005, Paris, France.

[d]Paul Scherrer Institut (PSI), Forschungsstrasse 111, 5232 Villigen PSI, Switzerland.

[e]The European Synchrotron (ESRF), 71 Avenue des Martyrs, F-38043 Grenoble, France.

[f]Institute for Integrative Biology of the Cell (I2BC), CEA, CNRS, Université Paris-Saclay, F-91191 Gif-sur-Yvette CEDEX, France.

[g]Sorbonne Université, Ecole Normale Supérieure, PSL University, CNRS UMR 7203, Laboratoire des BioMolécules (LBM), 4 place Jussieu, F-75005 Paris, France.

*Corresponding author: sophie.combet@cea.fr

KEYWORDS

membrane protein, small-angle scattering (SAXS/SANS), MALLS, SDS, DPC, DMPC, mouse TSPO

HIGHLIGHTS

• DMPC promotes the refolding of mTSPO by improving its 2D and 3D structural reorganization

• The amphiphilic belt of mTSPO is more extended in DMPC:DPC than in DPC and SDS

• The aggregation of mTSPO is reduced in DMPC:DPC compared to DPC

• mTSPO is stable in DMPC:DPC mixtures for structure/function studies in solution

• mTSPO affinity for ligands is higher in DMPC:DPC than in DPC and SDS

ABBREVIATIONS

CD, circular dichroism; DDM, dodecyl maltoside; DM, decyl maltoside; DMPC, 1,2-dimyristoyl-sn-glycero-3-phosphocholine; DPC, dodecyl phosphocholine; MALLS, multi-angle laser light scattering; MST, microscale thermophoresis; mTSPO, mouse TSPO; SANS, small-angle neutron scattering; SAXS, small-angle X-ray scattering; SDS, sodium dodecyl sulfate; SEC, size-exclusion chromatography; SLD, scattering length density; Trp, tryptophan; TSPO, translocator protein.

Enhanced structure/function of mTSPO

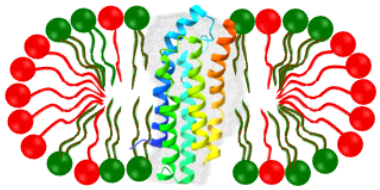

DMPC:DPC

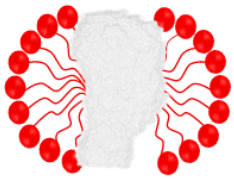

DPC

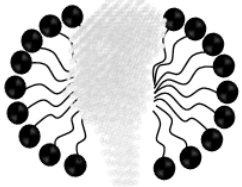

SDS

SAXS (Rg and Dmax)

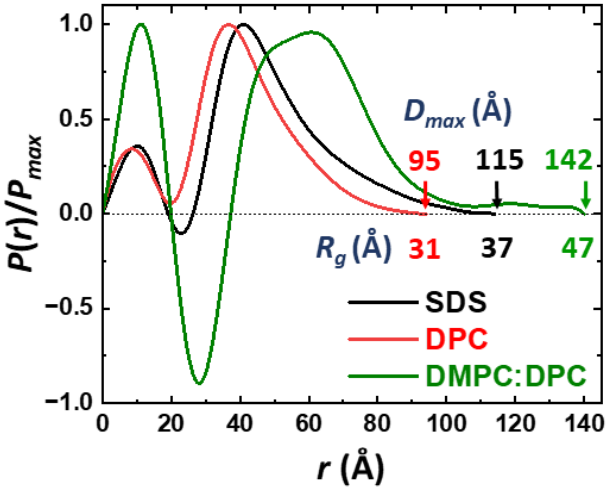

MST (ligand affinity)

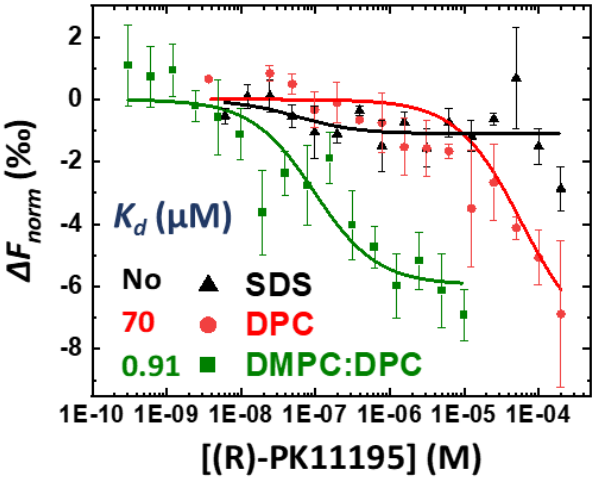

ABSTRACT

TSPO is a ubiquitous transmembrane protein used as a pharmacological marker in neuroimaging. The only known atomic structure of mammalian TSPOs comes from the solution NMR assignment of mouse TSPO (mTSPO) bound to the PK11195 ligand and in a DPC surfactant environment. No structure is available in a biomimetic environment and without PK11195 which strongly stiffens the protein.

We measured the effect of different amphiphilic environments on ligand-free mTSPO to study its structure/function and find optimal solubilization conditions. By replacing the SDS surfactant, where the recombinant protein is purified, with mixed lipid:surfactant (DMPC:DPC) micelles at different ratios (0:1, 1:2 and 2:1, *w*:*w*), the α-helix content and interactions and the intrinsic tryptophan (Trp) fluorescence of mTSPO are gradually increased.

SAXS analysis shows a more extended mTSPO/belt complex with the addition of lipids: D_{max} ~95 Å in DPC alone *versus* ~142 Å in DMPC:DPC (1:2). SEC-MALLS shows that the molecular composition of the mTSPO belt is ~98 molecules for DPC alone and ~58 DMPC and ~175 DPC for DMPC:DPC (1:2). Additionally, DMPC:DPC micelles stabilize mTSPO compared to DPC alone, where the protein has a greater propensity to aggregate. These structural changes are consistent with the increased affinity of mTSPO for the PK11195 ligand in the presence of lipid (K_d ~70 μM in DPC alone *versus* ~0.91 μM in DMPC:DPC, 1:2), as measured by MST.

In conclusion, the use of mixed lipid:surfactant micelles opens new possibilities for stabilizing membrane proteins for their study in solution in a more biomimetic amphiphilic environment.

1. Introduction

The translocator protein (TSPO) is a functionally important and highly conserved transmembrane protein[1], mainly found in the outer mitochondrial membrane of mammals[2]. It was discovered almost 50 years ago and named the "peripheral benzodiazepine receptor" (PBR)[3]. In 2006, the name was changed to "translocator protein" in reference to the subcellular localization and function of the protein[4]. However, the exact role of this protein is still unclear, although many biological functions have been attributed to TSPO, such as the transport of cholesterol and porphyrins and roles in steroidogenesis, energy metabolism, and neurogenesis[4,5].

TSPO is a tryptophan (Trp) rich protein (containing 12 Trp residues) made of five transmembrane α-helices[6,7]. Two ligand binding sites are present, consisting in (*i*) one pocket between its five α-helices able to bind both natural and synthetic ligands[8–11] and (*ii*) a cholesterol-recognition amino acid consensus (CRAC) binding site at the C-terminus of its 5th helix[12]. Thanks to its high affinity to many drug ligands, TSPO has been for a while a biomarker of strong pharmacological interest[12]. It is widely used in neuroimaging for many inflammatory, cancerous, and neurodegenerative diseases, especially in positron emission tomography scans[13].

The only known atomic structure for mammalian TSPOs is the NMR structure of mouse (*Mus musculus*) TSPO (mTSPO), solved in dodecylphosphocholine (DPC) detergent and in presence of the pharmacological ligand (R)-PK11195, which strongly stiffens the protein[8]. However, this structure is controversial since DPC is known to destabilize proteins[14]. Above all, without ligand, the apo-state protein is very flexible and its structure has not yet been solved, neither in detergent[15], or in membrane[16]. Therefore, all attempts to obtain an atomic structure of a ligand-free mTSPO under native conditions have failed so far. Resolving the atomic structure of TSPO in mammals therefore remains a challenge to better understand its affinity and interaction with ligands in order to develop new drug ligands for diagnosis and therapy [13,17].

Two high-resolution crystallographic structures are known for bacterial TSPOs (*Rs*TSPO[10] and *Bc*TSPO[9]). These bacterial TSPOs were solubilized and purified in nonionic

decyl or dodecylmaltoside (DM or DDM) and crystallized in a membrane-like lipidic cubic phase [9,10]. In contrast, recombinant mTSPO has so far been produced in *E. coli*, a non-mitochondrial environment, and solubilized by sodium dodecyl sulfate (SDS) from inclusion bodies[18,19]. In contrast to mTSPO[8,15], no major structural difference was observed for bacterial TSPOs with and without ligand[20], although bacterial TSPOs and mTSPO have a high sequence identity (30-35%), even higher than between bacterial TSPOs themselves (23%)[20]. These conformational differences between mammalian and bacterial structures, as well as their ability to be solubilized and crystallized, may be due to the amphiphilic environment used to solubilize and purify these proteins[14], as well as the protein sequence.

Local structure of free-ligand mTSPO, as revealed by circular dichroism (CD) and intrinsic Trp fluorescence, is strongly sensitive to its amphiphilic environment[18,19]. By combining SANS and the contrast-matching technique with *ab initio* modeling, we showed recently that mTSPO 3D conformation is partially unfolded and flexible in SDS, while in DPC the protein is much more compact and structured but still significantly different from the PK-binding NMR structure[18]. The protein amphiphilic environment affects also the affinity of mTSPO for ligands: in SDS, mTSPO cannot bind any ligand[19], whereas after exchanging to DPC detergent, a binding affinity was observed related to the helical structuration of the protein[7,21,22]. Furthermore, mTSPO recovers higher affinities for PK11195 and cholesterol ligands when reconstituted in proteoliposomes, a more native-like environment compared to detergent micelles[17]. Solid-state NMR studies of mTSPO in liposomes suggested that lipids may facilitate the conformational flexibility of mTSPO to enhance its recognition and interaction for ligands and other protein partners[16].

Here, we study the effect on the structure/function of mTSPO of a more biomimetic environment by using DMPC (1,2-dimyristoyl-sn-glycero-3-phosphocholine):DPC (dodecylphosphocholine) mixed “micelles” at different ratios (0:1, 1:2, and 2:1). Phosphatidylcholine (PC) represents 54% of the lipids of the outer mitochondrial membrane in

mammals where TSPOs are mainly localized[24]. We use the term "micelles" for the present study although it is debatable, since such systems have also been described as "binary complexes"[25]. Moreover, DMPC lipids, with a melt transition (T_m) of 24°C, have the advantage to be fluid at physiological temperatures compared to other PC lipids[26]. We used combined DMPC:DPC micelles since the two molecules share not only the same head group but almost the same chain length (~12 carbons). Combinations of lipid:surfactant mixtures are known to influence the refolding, stability, and function of membrane proteins, like for bacteriorhodopsin reconstitution in DMPC:CHAPS micelles[27]. In addition, such mixed systems represent a physiologically relevant environment to obtain the solution structures of membrane proteins by small-angle scattering (SAS) techniques and provide good starting conditions for crystallization[14,28].

2. Materials & Methods

2.1. Materials

All salts for buffers were purchased from Sigma-Aldrich. Sodium dodecyl sulfate (SDS, CAS number 151-21-3, Sigma-Aldrich) and dodecyl phosphocholine (DPC, CAS number 29557-51-5, CliniSciences) detergents were used above their respective critical micelle concentrations (CMC). Mixed micelles of DMPC:DPC, using 1,2-dimyristoyl-sn-glycero-3-phosphocholine phospholipid (DMPC, CAS number 18194-24-6, Avanti polar lipids), were prepared at 1:2 and 2:1 ratios (*w*:*w*) at least one week before experiments to ensure a good solubilization by mixing powders directly in buffers containing 50 mM HEPES, pH 7.8, and 150 mM NaCl. A film of the fluorescent probe-labeled nitrobenzoxadiazole-1,2-dimyristoyl-sn-glycero-3-phosphoethanolamine (NBD-DMPE, CAS number 474942-82-0, Avanti polar lipids) was prepared and rehydrated with the mixed micelle solution for purification and lipid quantification. Structure and parameters of the detergents and lipids used in the present study are shown in Tables S1 & S2 in the Supporting Information (SI).

2.2. Expression and purification of mouse TSPO (mTSPO)

6His-tagged mTSPO was cloned into pET15 plasmid and overexpressed in BL21 (DE3) *Escherichia coli* bacteria. The protein was extracted by affinity chromatography (HisTrap, Cytiva) from bacterial inclusion bodies using 1% SDS, as previously described [29]. During the new purification protocol developed in the present study, the belt-exchange process with DMPC:DPC mixtures was evaluated at each step by the absorbance spectrum of the NBD-DMPE probe at its two maxima, at 335 and 465 nm. This probe was added at a molar ratio of 1:100 of DMPC concentration. The purification buffers were 50 mM HEPES, pH 7.8, 150 mM NaCl. The wash and exchange buffers contained 3 mM imidazole and the elution buffer was supplemented with 300 mM imidazole. mTSPO expression levels were quantified using absorption measured at 280 nm with the extinction coefficient of 3.88 mg/mL, calculated from the amino acid sequence composition of mTSPO containing also the six histidines from the tag. DMPC quantification was deduced from the NBD absorbance using its calibration curve (Fig. S1, A-B).

2.3. Quality control of the purified mTSPO

To provide valuable information about the purity and quality of the purified protein, mTSPO was analyzed by SDS-PAGE (12% acrylamide, Biorad) and by size exclusion chromatography (SEC) coupled to the multiple-angle laser light scattering (SEC-MALLS). SEC-MALLS analysis of mTSPO in DMPC:DPC complex was carried out using Superdex Increase 75 (10/300), 24 mL column (Cytiva). The Shimadzu high performance liquid chromatography (HPLC) system was coupled to three detectors: (*i*) a UV-VIS detector SPD-20A (Shimadzu) to measure the absorbance at 280 nm, (*ii*) an Optilab® T-rEX refractometer to measure the differential refractive index (d*RI*), and (*iii*) a miniDawn® TREOS detector (Wyatt Technology) to measure the static light scattering (LS) intensity at three scattering angles (44, 90, and 136°). The Superdex column was equilibrated with a mobile phase containing 50 mM HEPES, pH 7.8, 150 mM NaCl, and 0.05% DMPC:0.1% DPC (*w*:*w*) at a flow rate of 0.3 mL/min. Addition of the

lipid:detergent mixture at the same ratio in the elution buffer is mandatory to avoid demicellization effects of the protein-bound amphiphiles, which would induce mTSPO aggregates and wrong estimation of mTSPO molar mass (Fig. S2, Table S3).

After UV, RI, and LS baseline stabilization and buffer subtraction, as well as interdetector delay (caused by the offset time between the three detectors) and peak-broadening corrections on a standard sample of known molar mass and monodisperse monomeric form[30] (*i.e.* injection of 25 µL of bovine serum albumin (BSA, Sigma) at 5 mg/mL, dissolved in the mobile phase), 25 µL of purified mTSPO/DMPC:DPC at 6 mg/mL (287.5 µM) was injected onto the column. Collected LS intensities at the three angles were analyzed using the Astra software (version 5.3.4.20, Wyatt Technology). The absolute molar mass of protein/lipid:detergent complex was calculated from the equation:

$$MW_{complex} = \frac{R(\theta)}{k \cdot \left(\frac{\partial n}{\partial c}\right)^2_{complex} \cdot c_{complex}} \qquad \text{Eq. 1}$$

where $c_{complex}$ is the concentration of the protein/lipid:detergent complex, $R(\theta)$ the Rayleigh ratio and k an apparatus constant. The complex concentration was obtained from absorbance and *RI* measurements knowing the extinction coefficients ($\varepsilon_{0.1\% \text{ at } 280 \text{ nm}}$) and *RI* increments ($\partial$n/$\partial$c) of both tagged 6His-mTSPO and DMPC:DPC micelles. Thus, we used for (*i*) tagged-mTSPO: $\varepsilon_{0.1\%}$ = 3.88 mL.mg^{-1}.cm^{-1} and ∂n/∂c = 0.197 mL.g^{-1} (obtained from SedFit software) and for (*ii*) DMPC:DPC micelles: $\varepsilon_{0.1\%}$ = 0 and ∂n/∂c DMPC:DPC = 0.114 ± 0.001 mL.g^{-1} (measured by injecting increasing concentrations of DMPC:DPC mixtures at 1, 4, 6, 8, and 10 g/L dissolved in 50 mM HEPES, pH 7.8, 150 mM NaCl, directly in the Optilab® T-rEX refractometer, Fig. S3). Respective mass fractions of mTSPO and bound lipid:detergent were calculated using the automatic procedure "Protein Conjugate" from Astra software (Table 1).

2.4. Far-UV circular dichroism (CD)

Circular dichroism (CD) measurements were recorded on a ChirascanPlus spectropolarimeter (Applied Photophysics). Spectra were measured from 185 to 280 nm (1 nm step) in 1-mm pathlength Hellma cells fixed at 20°C. For titration measurements, we used mTSPO purified in 0.2% SDS in 50 mM HEPES, pH 7.8, 150 mM NaCl, 300 mM imidazole, and then dialyzed against 10 mM phosphate buffer, pH 7.8, 0.2% SDS to eliminate salts and imidazole. Spectra were first recorded at the initial protein concentrations of 5 µM (~0.1 mg/mL). Increasing concentrations of DMPC:DPC micelles (at 0:1, 1:2, and 2:1 ratios) were added to the mTSPO-0.2% SDS sample.

For all measurements, blanks corresponding to the measurements of micelles alone in the buffer were subtracted, dilution effect was corrected, and the results from two similar independent measurements were averaged and normalized to the protein concentration. Data were smoothed and deconvoluted using BeStSel software[31] (http://bestsel.elte.hu/) to estimate the secondary structure content of mTSPO, especially the percentage of helicity. The ratio of ellipticity measured at 222 and 208 nm $\left(\frac{\Delta\varepsilon_{222\,nm}}{\Delta\varepsilon_{208\,nm}}\right)$ was used as an indicator of degree of "coiled-coils" and helical interactions. For all titrations, graphs were plotted as function of DPC concentration to compare the results with each other.

The following equation was used to calculate the semi-saturation (*SS*) value of the titration curve:

$$Y = \frac{[DPC]*Y_{max}}{SS+[DPC]} \qquad \text{Eq. 2}$$

where *Y* corresponds to, either $\left(\frac{\Delta\varepsilon_{222\,nm}}{\Delta\varepsilon_{208\,nm}}\right)$ ratio, or helicity content, and Y_{max} corresponds to *Y* at the DPC concentration used to reach the plateau. Fitting of the data was made using Eq. 2 in Kaleigraph software.

2.5. Tryptophan (Trp) intrinsic fluorescence

The emission spectra of the intrinsic fluorescence of Trp for mTSPO (which contains naturally 12 Trp amino acids) were recorded on Eclipse spectrofluorometer (Cary) instrument while gradually increasing the emission wavelength between 310 and 500 nm (bandwidth of 2 nm, 1 nm step, 0.1 s/nm), and keeping a constant excitation wavelength of 290 nm (bandwidth of 2 nm) in 10-mm pathlength quartz Hellma cells, under agitation at 20°C.

Like for CD, for titration measurements, we used mTSPO purified in 0.2% SDS in 50 mM HEPES, pH 7.8, 150 mM NaCl, 300 mM imidazole, and then dialyzed against 10 mM phosphate buffer, pH 7.8, 0.2% SDS to eliminate salts and imidazole. Spectra were first recorded at the initial protein concentrations of 2.5 µM (~0.05 mg/mL). Then, increasing concentrations of DMPC:DPC micelles (at 0:1, 1:2, and 2:1 ratios) were added to the mTSPO-0.2% SDS samples and spectra recorded at each concentration.

For all measurements, blanks corresponding to the measurements of micelles alone in the buffer were subtracted, dilution effect was corrected, and the results from two similar independent measurements were averaged and normalized to the protein concentration. For all titrations, graphs were plotted as function of DPC concentration to compare the results with each other.

The following sigmoid equation was used to fit the data and determine the half-maximal effective concentration (EC_{50}) value of the titration curve:

$$Y = Y_{max} + \frac{(Y_{min} - Y_{max})}{1 + \left(\frac{[DPC]}{EC_{50}}\right)^{k}} \qquad \text{Eq. 3}$$

where Y corresponds to $\frac{\Delta(F_c - F_0)}{F_{max} - F_0}$, where fluorescence is measured at λ = 335 nm (*i.e.* the wavelength of the maximum intensity of emission fluorescence) with F_c the fluorescence intensity for a given [DPC], F_0 the fluorescence intensity for [DPC] = 0, and F_{max} the fluorescence intensity for [DPC] used to reach saturation. Y_{min} corresponds to the fluorescence intensity before adding DPC micelles. Y_{max} corresponds to the fluorescence intensity for DPC

concentration used to reach the plateau. *k* corresponds to the slope of the sigmoid curve. Fitting of the data and EC_{50} determination were made using Eq. 3 in Kaleigraph software.

2.6. Dynamic light scattering (DLS)

Dynamic light scattering (DLS) was performed to obtain the hydrodynamic size distribution of mTSPO in different amphiphilic environments. Measurements were performed using a DynaProPlate Reader 3 (Wyatt) instrument. A volume of 20 µL of mTSPO/SDS, mTSPO/DPC, and mTSPO/DMPC:DPC complexes, at 6.5, 5.2, and 4.3 mg/mL respectively, in a buffer containing 50 mM HEPES, pH 7.8, 150 mM NaCl supplemented with free micelles, was loaded in a 384-well microplate (Corning ref 3540, New-York, USA). Each sample was measured three times at 20°C using a setup of 10 acquisitions of 5 sec after spinning at 27,000 g for 15 min at 4°C. Measurements were analyzed with the DYNAMICS version V7.10.0.21 software provided with the equipment (Wyatt, Santa Barbara, CA, USA).

2.7. Small-angle neutron scattering (SANS)

SANS experiments were performed on SANS-I instrument (PSI, Villigen, Switzerland) to measure mTSPO in contrast-matched environment using a wavelength of λ = 6 Å and a sample-to-detector distances of 1.6, 6, and 18 m. We measured overnight, at room temperature and in batch condition, using Hellma cells of 1 mm pathlength, mTSPO in 0.05% d-DMPC:0.1% d-DPC (1:2 ratio) in 100% D_2O buffer containing 50 mM HEPES, pD = 8.2 (pH 7.8), and 150 mM NaCl. The matching-out of d-DMPC in this buffer was checked experimentally (Fig. S4) and for d-DPC we used a mixture of 86% d-DPC:14% h-DPC to contrast match it in 100% D_2O buffer, as already described[18].

Data analysis was made using SasView software (https://www.sasview.org/). mTSPO in DMPC:DPC can be fitted with the "polymer with excluded volume" model[32], which generalizes the Debye model for the Gaussian chain. This model describes the scattering from polymer chains

subject to excluded volume effects and corresponds here to a denaturated conformation of mTSPO protein. In this model, the radius of gyration R_g is defined as:

$$R_g^2 = \frac{a^2 n^{2\nu}}{(2\nu+1)(2\nu+2)} \qquad \text{Eq. 4}$$

where ν is the excluded volume parameter and is related to the Porod exponent m (*i.e.* the slope) since $\nu = 1/m$, a is the size of the base unit (*i.e.* amino acid residues), and n is the degree of polymerization (*i.e.* the number of residues in the protein chain).

The best fit found for mTSPO in DPC environment is the "mass fractal" model (see Mildner & Hall[33] for the equation), which calculates the scattering from fractal-like aggregates.

2.8. Small-angle X-ray scattering (SAXS) and SEC-SAXS

To study DMPC:DPC mixed micelles, SAXS experiments were performed using the SAXS laboratory beamline XEUSS 2.0 (XENOCS, Grenoble, France) equipped with a Pilatus detector (1 M) at LLB (Saclay, France). The measurement wavelength was λ = 0.154 nm (CuKα) and the Q-range was 2 10^{-2}-1 $Å^{-1}$. Samples of DMPC:DPC mixed micelles at ratios 2:1, 1.5:1, 1:1, 0.5:1, 0.25:1, and 0:1 were measured in Kapton capillaries (1.5 mm of diameter) at room temperature for 2 h of acquisition *per* sample.

SEC-SAXS experiments of mTSPO in 0.05% DMPC:0.1% DPC were performed on the BioSAXS beamline BM29 (ESRF, Grenoble, France)[34] at the Q-range 5.5 10^{-3} - 0.5 $Å^{-1}$. Sample volumes were injected into the Superdex 75 (10/300) increase column (24 mL), pre-equilibrated with three column volumes of buffer containing 50 mM HEPES buffer, pH 7.8, 150 mM NaCl, and 0.05% DMPC:0.1% DPC at a flow rate of 300 µL.min^{-1} and a fixed temperature of 20°C. SEC-SAXS images were collected during the elution with a duration of 4 sec *per* frame. The 2D-SAXS patterns were normalized and averaged using the automated data processing pipeline available at BM29[34]. The first frames corresponding to the elution buffer were averaged using Scatter software[35]. For each injected protein amount, frames having a stable range for the radius of gyration (R_g) during the elution peak were selected and buffer-subtracted, to eliminate the

contribution of the free mixed micelles in solution, and then averaged to get the intensity $I(Q)$ as a function of the modulus of the scattering vector Q, where $Q = \frac{4\pi}{\lambda}\sin(\theta)$ with λ the X-ray (XR) wavelength and θ half of the angle between incident and scattered XR beams (Fig. S5). Analysis of SAXS curves was performed using RAW software[36] to access to $I(Q)$, R_g, $I(0)$, and the pair-distance distribution function $P(r)$ in real space to get the maximal distance D_{max}.

2.9. Microscale thermophoresis (MST)

MST experiments were performed using the Monolith NT.115 instrument. mTSPO, solubilized in SDS, DPC, or DMPC:DPC (1:2), was labeled using the Monolith NT™ Protein Labeling Kit BLUE–NHS. Following the manufacturer instruction (Cat No. MO-L003, NanoTemper Technologies), the N-hydroxysuccinimide (NHS) coupling the blue fluorescent dye NT-495 reacted efficiently with primary amines of mTSPO lysines to form highly stable dye-protein conjugates. A concentration of 10 nM of labeled mTSPO was mixed with increased concentration of (R)-PK11195 ligand (CAS number 205934-46-9) in 50 mM HEPES, pH 7.8, and 150 mM NaCl supplemented with SDS, DPC, or DMPC:DPC free micelles. All samples contained at the end 1% of DMSO used for solubilizing the ligand. They were then loaded into 16 standard capillaries. The experiments were performed with 40% MST power at 20°C. The data were analyzed using the MO Affinity Analysis software (version 2.3, Nanotemper) and K_d values were obtained from duplicate/triplicate experiments, using the following equation (Eq. 5):

$$f(c_{\text{ligand}}) = Unbound + (Bound - Unbound).\frac{c_{\text{ligand}} + c_{\text{target}} + K_d - \sqrt{(c_{\text{ligand}} + c_{\text{target}} + K_d)^2 - 4 . c_{\text{ligand}} . c_{\text{target}}}}{2c_{\text{target}}}$$

where $f(c_{\text{ligand}})$ corresponds to the F_{norm} value at a given ligand concentration (c_{ligand}), *Unbound* is the F_{norm} signal of the target alone, *Bound* is the F_{norm} signal of the complex, K_d is the dissociation constant or binding affinity, and c_{target} is the final concentration of target in the assay.

3. Results & Discussion

3.1. Purification of mTSPO in DMPC:DPC micelles

We developed an innovative procedure to exchange the mTSPO belt from SDS to DMPC:DPC lipid:detergent mixtures using two exchange steps. This process occurs after washing the column 3 times with 2% DPC (2 mL each) while the protein remains immobilized on Ni-NTA chelation resin (~0.8 mL) (Qiagen, Les Ulis, France) (Fig. S1C). The initial step (*i*) entails six exchanges of 1.5 mL each with 0.4% DMPC:0.2% DPC (2:1, *w*:*w*) to fully form ternary complexes, while the second (*ii*) corresponds to three exchanges of 1.3 mL each with 0.05% DMPC:0.1% DPC (1:2, *w*:*w*) to reduce the quantity of lipids and consequently lower the sample cost especially in SEC condition, that requires large volume to equilibrate the column. As the exchange buffer containing mixed micelles passes through the nickel column, the exchange was tracked by specifically measuring the absorbance of NBD-DMPE probe (fixed to the mixed micelles) at 465 nm in the flow-through samples collected at each intermediate step.

An immediate exchange of detergent micelles surrounding the immobilized mTSPO was observed upon introducing lipids in the exchange buffer containing 0.4% DMPC:0.2% DPC (*w:w*) micelles, evidenced by the NBD absorbance decrease at 465 nm between the buffer and the first collected flow-through fraction (Fig. S1D). With successive exchanges, the NBD-DMPE absorbance in the collected flow-through fractions increase progressively, showing the different stages of completing the exchange process until reaching a plateau (in the last two collected flow-through fractions), at a level nearly equivalent to the buffer (Fig. S1D, inset). NBD absorbance did not reach exactly the same level at this plateau compared to the buffer, which suggests possible interactions of the mixed micelles with the Ni-NTA chelation resin and/or with the immobilized mTSPO/DMPC:DPC complex.

The same strategy was employed at the second step of the protocol to track the exchange of lipids between the free mixed micelles in solution and the belt of mTSPO. The NBD absorbance of the flow-through fractions decreased progressively with the exchange buffer containing 0.05%

DMPC:0.1% DPC (*w:w*), *i.e.* the quantity of lipids decreased in the free mixed micelles, as well as in the protein belt (see 3.2. paragraph in the Results section). To achieve a perfect exchange and washing of the column, three exchange steps were necessary, as expected and confirmed by the superposition of the absorption spectra of the third flow-through collected fraction with the buffer containing 0.05% DMPC:0.1% DPC (*w:w)* (Fig. S1E).

SDS-PAGE analysis shows that purified mTSPO is nearly pure, with very few contaminants (Fig. 1A). Absorbance of the protein fractions shows a maximum at 280 nm attributed to the protein aromatic residues, with a typical shoulder at 290 nm corresponding more specifically to Trp residues (Fig. 1B). This confirms that mTSPO containing 12 Trp residues was dominant in the elution fractions, and its concentration was deduced from absorption at 280 nm (Fig. 1C). Using NBD-DMPE absorption at 465 nm and its molar excitation coefficient (ε = 0.07 mL μg^{-1} cm^{-1}), obtained from the slope of the calibration curve (Fig. S1, D-E), together with the molar ratio of 1:100 of NBD:DMPC, we measured the concentration of DMPC bound to mTSPO (Figs. S1F & 1C). Thus the calculated mTSPO:DMPC ratio was 1:9 (*w*:*w*), using their respective molecular weights (MW_{mTSPO} = 20,870 g/mol, MW_{DMPC} = 677.93 g/mol). This corresponded to 58 ± 1 molecules of DMPC *per* mTSPO belt.

We concluded that this protocol of belt exchange of mTSPO is effective, resulting in pure mTSPO/belt complex. Membrane proteins, known for their pronounced affinity for lipids over detergents, have a tendency to associate strongly with lipids, explaining the rapid and effective exchange of mTSPO/detergent belt to a lipid:detergent mixed belt. Such exchange provides an amphiphilic environment that is more biomimetic because it better mimics the natural cellular membrane.

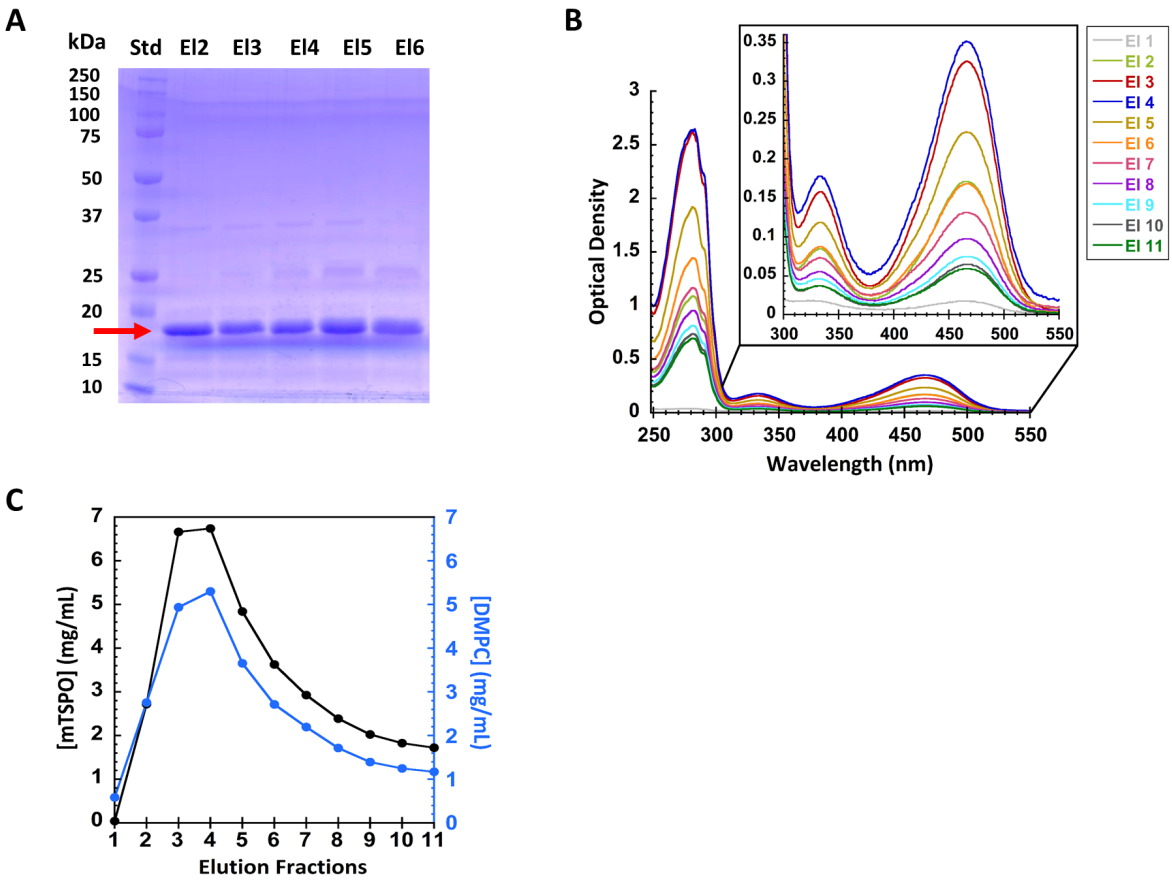

Figure 1. (***A***) SDS-PAGE (12%) of elution fractions (from El-2 to El-6) collected during mTSPO (red arrow) purification on Ni-NTA resin. The blue line below mTSPO protein bands is attributed to light artifact while scanning the gel. **(*B*)** Absorbance spectra of mTSPO elution fractions with 0.05% DMPC:0.1% DPC coupled with 0.0005% NBD-DMPE, noted from El-1 to El-11 (see Fig. S1C for protocol details). The maximum at 280 nm corresponds to mTSPO absorption and the maxima at 335 and 465 nm correspond to that of NBD-DMPE probe. **(*C*)** Concentration of mTSPO and of its associated DMPC lipids as function of elution fractions. DMPC concentration is deduced from NBD probe concentration (see text for details).

3.2. Quality control of mTSPO/DMPC:DPC complex

Prior to characterizing and studying protein solution structure using biophysical and scattering approaches, it is crucial to assess homogeneity, oligomeric state, and mass of protein sample, to enhance data quality and analysis. SEC-MALLS showed two distinct peaks for mTSPO/DMPC:DPC complex, indicating the coexistence of both protein multimers/aggregates

between 40 and 90 kDa and monomers of about 22 kDa, in good agreement with the expected *MW* of the recombinant 6His-tagged protein (~21 kDa) (Fig. 2). Free mixed micelles co-elute with mTSPO monomer (at ~8.3 mL and ~8.5 mL, respectively), as shown by the corresponding calculated masses after injecting a higher concentration of mixed micelles (0.25% DMPC:0.5% DPC) with the same 1:2 ratio (Fig. 2). Despite this, since their concentration in the studied samples was much lower (1/5) and similar to that of the mobile phase (*i.e.* the subtracted buffer at 0.05% DMPC:0.1% DPC), their contribution was considered as negligible thereafter. From SEC-MALLS analysis, the masses of mTSPO/belt complex and bound DMPC:DPC belt were obtained (Fig. 2, Eq. 1). Considering NBD-DMPE probe quantification and *MW* of each amphiphilic component (MW_{DMPC} = 677.93 g/mol, MW_{DPC} = 351.5 g/mol), we deduced that ~175 DPC molecules were associated to mTSPO (Table 1). By comparing to our previous results on mTSPO, the DMPC:DPC belt associated to mTSPO (~233 molecules) is significantly larger than the detergent belts composed of SDS or DPC only (135 and 98 molecules, respectively)[18]. The ratio of DMPC:DPC in the belt is therefore equal to 1:1.6, which could be the optimal ratio for DMPC:DPC belt bound to mTSPO protein. This ratio is intermediate between the 2:1 ratio (0.4% DMPC:0.2% DPC (*w:w*)) of the first exchange buffer and the 1:2 ratio (0.05% DMPC:0.1% DPC (*w:w*)) used for the second step of exchange (Fig. S1C).

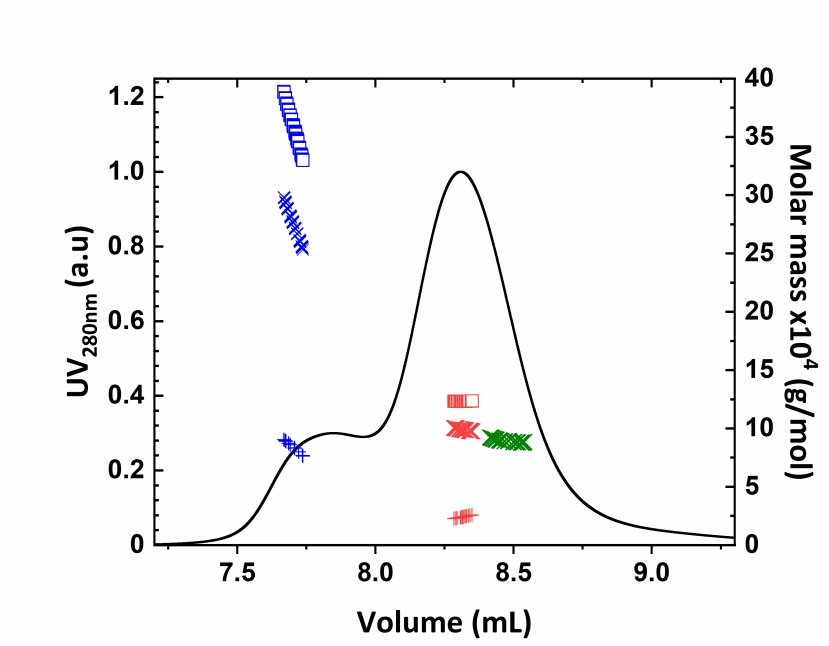

Figure 2. SEC-MALLS curve and analysis of mTSPO/DMPC:DPC ternary complex (blue: multimers/aggregates, red: monomers) and 0.25% DMPC:0.5% DPC mixed micelles (green). UV at 280 nm profiles of mTSPO/DMPC:DPC and mixed micelles were eluted using a Superdex 75 increase (10/300) column. Molar masses (*MW*) were calculated and depicted for mTSPO/lipid:detergent complex (□), mTSPO protein (+), and its bound lipid:detergent belt or mixed micelles (x). Note that the free mixed micelles do not absorb at 280 nm, so only their calculated molar mass is shown in green.

Table 1. Evaluation of the composition of mTSPO/DMPC:DPC complex from SEC-MALLS and NBD fluorescence analysis (MW_{DMPC} = 677.93 g/mol, MW_{DPC} = 351.5 g/mol).

	mTSPO/DMPC:DPC
mTSPO/DMPC:DPC complex molar mass (kDa)	123.3 ± 0.1
mTSPO protein molar mass (kDa)	22.3 ± 0.1
bound DMPC:DPC belt molar mass (kDa)	101.0 ± 0.1
number of bound DMPC lipid molecules (N_{DMPC})	58 ± 1
number of bound DPC detergent molecules (N_{DPC})	175 ± 1

3.3. Effect of DMPC lipids on mTSPO helical refolding

The transition from a SDS belt, where mTSPO is partially unfolded[18], to a DPC or DMPC:DPC belts induced significant changes in mTSPO far-UV CD spectra, with an increase in the maximum around 190 nm and a decrease at 210-240 nm range (Fig. 3, A-C). DMPC:DPC at 1:2 and 2:1 (*w*:*w*) ratios induced a larger increase in mTSPO helical content, from 27% to 42% and 45% respectively, compared to the addition of DPC micelles alone (helical content increasing from 27% to 40%) (Fig. 3D, Table S4). These fitting parameters correspond to the plateau value obtained at ~12 mg/mL of addition of DMPC:DPC at the three ratios. This increase is mainly attributed to the lipid properties providing a more favorable native-like environment promoting

mTSPO refolding. However, the helical content remains lower than the theoretical corresponding value (71%) calculated using SESCA software[37] from 6His-mTSPO AlphaFold model[18], suggesting that the refolding of mTSPO in DMPC:DPC environment remains different from the native folding of the protein. A similar value of ~70% is deduced from the NMR structure in presence of PK11195 ligand[15], whereas mTSPO has been described as highly flexible without ligand. Moreover, BeStSel analysis gives β-sheet content that has never been observed for any TSPO, suggesting to be careful with such analysis. The *SS* (semi-saturation, *i.e.* at the inflection point) values for helicity are 1.6, 0.8, and 1.2 mg/mL for DMPC:DPC at 0:1, 1:2, and 2:1 ratios (*w*:*w*), respectively, without significant difference (Fig. 3D).

The *SS* values obtained from the curve fitting (Fig. 3E, Eq. 2) are 0.75, 1.45, and 7.15 mg/mL at 0:1, 1:2, and 2:1 ratios of DMPC:DPC (*w*:*w*), respectively, showing a significant increase in DMPC:DPC (2:1) condition. A large increase in $\left(\frac{\Delta\varepsilon_{222\,nm}}{\Delta\varepsilon_{208\,nm}}\right)$ is observed at this latter condition (Table S4), which indicates stronger inter-helical interactions within mTSPO in presence of lipids. Moreover, the $\left(\frac{\Delta\varepsilon_{222\,nm}}{\Delta\varepsilon_{208\,nm}}\right)$ ratio obtained using the AlphaFold model[18] of mTSPO and DMPC:DPC (2:1) experimental data are similar (Table S4). This suggests a folding of mTSPO in DMPC:DPC (2:1) close to the folding found for this protein by AlphaFold, despite a different content of secondary structures (Table S4).

The presence of DMPC phospholipid in mixed micelles, which are major components of biomembranes, enhances the structuration of mTSPO transmembrane α-helices and their hydrophobic interactions, leading to a more structured and organized protein. Indeed, lipids are known to interact with specific regions of membrane proteins, inducing stabilization of helical structures[38].

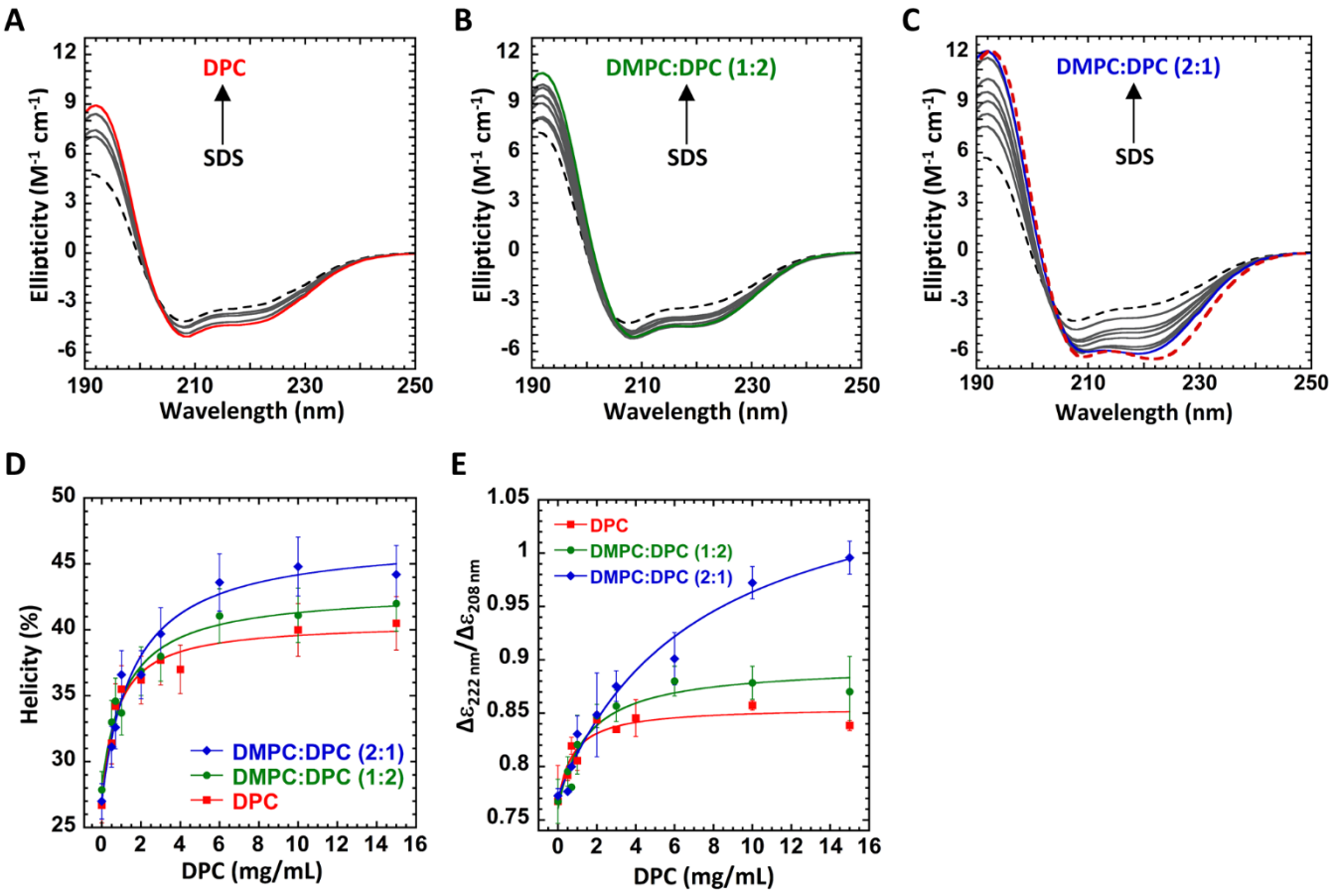

Figure 3. Changes of mTSPO secondary structures from SDS to DPC or DMPC:DPC environment. CD spectra of mTSPO (5 µM) purified in 0.2% (2 mg/mL) SDS (black dash line) and function of increasing concentrations of DMPC:DPC mixed micelles at the following ratios (*w*:*w*): **(*A*)** 0:1 (DPC alone), with concentrations at 0.05, 0.07, 0.1, 0.2, 0.3, 0.4, and 1% (grey lines), and finally at 1.5% (red line); **(*B*)** 1:2, with concentrations at 0.075, 0.105, 0.15, 0.3, 0.45, 0.9, and 1.5% (grey lines), and finally at 2.25% of total lipid:detergent (green line); **(*C*)** 2:1, with concentrations at 0.15, 0.21, 0.3, 0.6, 0.9, 1.8, and 3% (grey lines), and finally at 4.5% of total lipid:detergent (blue line). Theoretical CD curve obtained from SESCA software using the AlphaFold model of 6His-mTSPO[18] is represented in red (dash line). Titration curves using Eq. 2 of **(*D*)** mTSPO α-helix content (using BeStStel software) and **(*E*)** $\left(\frac{\Delta\varepsilon_{222\ nm}}{\Delta\varepsilon_{208\ nm}}\right)$ as function of DPC concentration, for the addition of DMPC:DPC at ratios 0:1, 1:2, and 2:1 (red, green, and blue full lines, respectively).

3.4. Effect of DMPC lipids on mTSPO intrinsic Trp fluorescence

The exchange of the SDS belt by DPC or by the mixture of DMPC:DPC induces a large increase in the intrinsic Trp fluorescence intensity of mTSPO. This increase is attributed to changes in the local environment of the 12 Trp residues, or at least part of them, distributed in the protein (Fig. 4, A-C). Fitting data with the sigmoid model gives an *EC*50 of 15, 14, and 6 mg/mL of DPC (Eq. 3), while titrating with, respectively, DMPC:DPC micelles at 0:1 (DPC alone), 1:2, and 2:1 ratios, respecively (Fig. 4D).

The *EC50* in intrinsic fluorescence is obtained for DPC concentrations higher than those observed to obtain the equivalent (*SS*) in CD, these measurements being performed for protein concentrations at the same order of magnitude (2 and 5 µM for fluorescence and CD, respectively). It means that the structuring of the helices "precedes" the local reorganization of the Trp residues, during the folding of mTSPO when exchanging SDS by the different ratios of DMPC:DPC (ratios 0:1, 1:2, and 2:1) (Fig. S6).

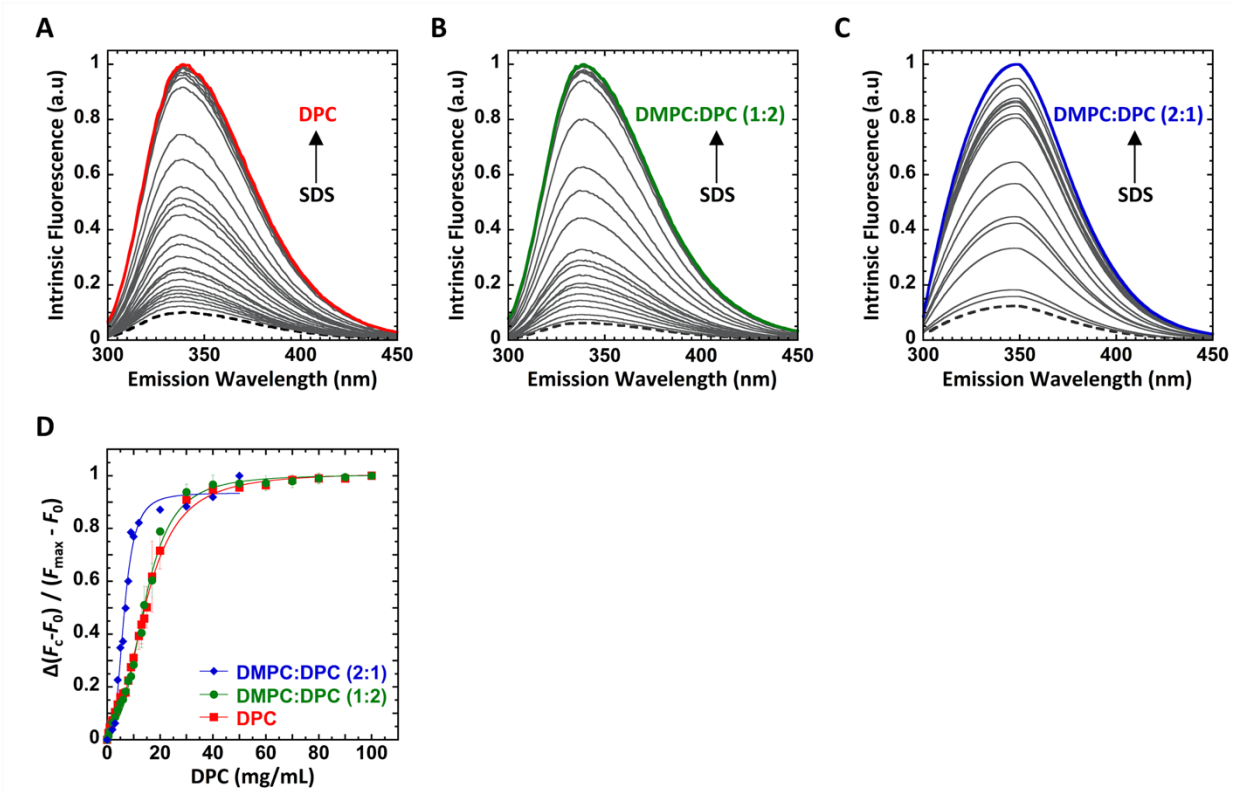

Figure 4. Increase in intrinsic Trp fluorescence intensity of mTSPO from SDS environment (black dash line) to increasing concentrations of the following ratios of DMPC:DPC micelles: **(*A*)** 0:1 ratio (DPC alone) at 0.5, 1, each 1 mg/mL from 2 to 10, 12, 13, 14, 15, 17, and each 10 mg/mL from 20 to the final concentration of 100 mg/mL (red line); **(*B*)** 1:2 ratio at 0.5, 1, 1.5 each 1 mg/mL from 2 to 10, 12, 13, 14, 15, 17, and each 10 mg/mL from 20 to the final concentration of 100 mg/mL of DPC concentration. The green line corresponds to the final concentration of 100 mg/mL of DPC **(*C*)** ratio 2:1, from 2 to 100 (each 1 mg/mL), then 12, 20, 30, 40, 50 mg/mL of DPC (blue line). **(*D*)** Titration curves of intrinsic fluorescence changes for mTSPO as function of DPC concentration for addition of DMPC:DPC (red squares, green disks, and blue diamonds for, respectively, ratios of 0:1, 1:2, and 2:0). Fitting of the experimental data is shown, using a sigmoid model (Eq. 3) (red, green, and blue lines, respectively, with corresponding χ^2 of 0.015, 0.019, and 0.025). For DMPC:DPC at ratios 0:1 and 1:2, results correspond to the average of two independent measurements. Only one measurement of DMPC:DPC at ratio 2:1 could be performed due to the high cost of DMPC.

3.5. Oligomeric/aggregated state of mTSPO/amphiphile complex

DLS was performed to compare the solubility of mTSPO in SDS, DPC, and DMPC:DPC (1:2) environments and to obtain the hydrodynamic size distribution of the complexes (Fig. 5). The size distribution analysis of the correlation function shows a clear first peak in DPC and DMPC:DPC, indicating a well-dispersed particle system in both conditions, consistent with monodisperse systems (Fig. 5, B-C, Table S5). In contrast, the size distribution in SDS appears extended, reporting a polydisperse system (Fig. 5A). The first peak is centered at R_h~2.65 nm in both SDS and DPC, whereas it is centered at R_h~1.3 nm in DMPC:DPC, highlighting a higher monodispersity in presence of lipids (Table S5).

In contrast, the size distribution of the second peak, corresponding to oligomeric and aggregated forms of the complex, is significantly wider for DPC compared to DMPC:DPC (1:2)

(68% *versus* 19% polydispersity, respectively) (Table S5). Moreover, the % of monomeric scatterers represent only ~84% in DPC, whereas they are roughly 100% in DMPC:DPC environment (Table S5), showing that the presence of lipids improves the solubility of mTSPO and reduces its aggregation, compared to DPC alone.

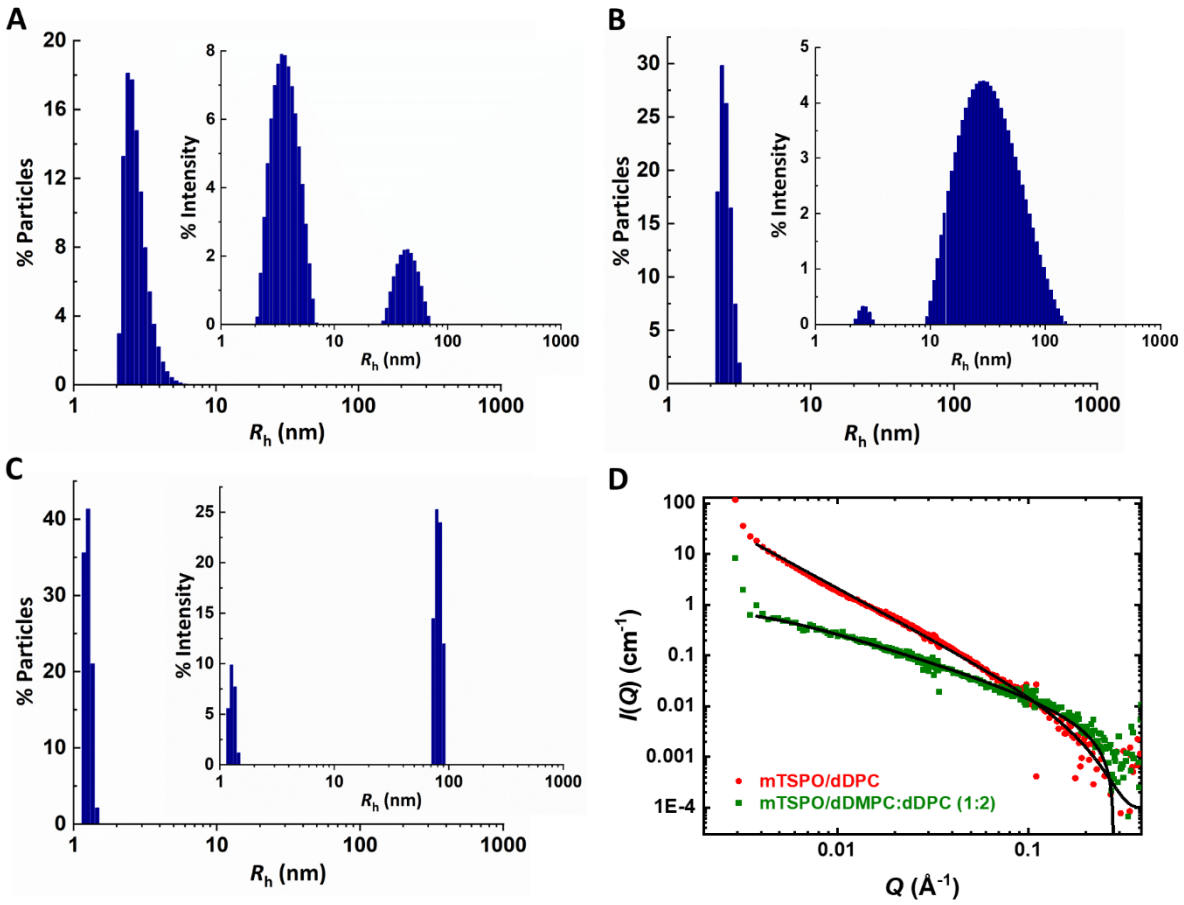

Figure 5. Size distribution of particles measured by DLS for (***A***) mTSPO/SDS, (***B***) mTSPO/DPC, and (***C***) mTSPO/DMPC:DPC (1:2, *w*:*w*) complexes, as function of the hydrodynamic radius (R_h) distribution. The insets represent the distribution of light scattering intensity as function of R_h distribution. (***D***) SANS curves measured in batch (SANS-I, PSI, Villigen, Switzerland) of mTSPO/dDPC (red) and mTSPO/dDMPC:dDPC (1:2, *w*:*w*) (green) complexes with respective contrast-matched belts, *i.e.* by probing specifically the protein scattering. Corresponding fits (black lines) using the "mass fractal" and "polymer excluded volume" models are shown for dDPC and dDMPC:dDPC environments, respectively.

3.6. Oligomeric/aggregated state of mTSPO protein

The solution structure of mTSPO was specifically measured using SANS and contrast matched dDPC and dDMPC:dDPC belts and free micelles. We determined that 100% of deuterated dDMPC are contrast matched in 100% D_2O buffer (Fig. S4), as well as a mixture of 86% dDPC/14% hDPC, as previously published[18].

The SANS curves of mTSPO in contrast-matched dDPC and dDMPC:dDPC (1:2) are significantly different, with slopes of 2.11 and 1.18, respectively (Fig. 5D). The SANS curve of mTSPO in dDMPC:dDPC can be fitted using the "polymer excluded volume" model, suggesting the protein is unfolded in this condition. We found that $\nu = 0.8426$, therefore Eq. 4 becomes: $a^2 n^{1.6852} = 9.895 * 303^2$. Using n = 188 amino acids for 6His-mTSPO sequence, a is found to be 11.6 Å, which is consistent with the order of magnitude of the dimension of an amino acid.

The best fit found for mTSPO in DPC environment is the "mass fractal" model, with a fractal dimension D_f = 2.02, and by imposing R (radius) = 11.6 Å, to be consistent with the fit of mTSPO in DMPC:DPC. However, this value does not play a role, because the lower cutoff is outside the SANS window measurement. This model is consistent with the presence of many multimers and aggregates of mTSPO in dDPC, as shown also by DLS on the whole complex in the corresponding DPC condition (Fig. 5B).

After SANS measurements (overnight at room temperature), the sample aspect was clearly different between the two amphiphilic conditions. The sample in dDPC was turbid, suggesting protein degradation, in contrast to the sample in dDMPC:dDPC which remained transparent (Fig. S7). This highlights that high protein concentrations used in scattering studies (several mg/mL) in dDMPC:dDPC mixed micelles cannot prevent denaturation of the protein over several hours. However, such mixture can stabilize mTSPO better than DPC alone by avoiding aggregation. Therefore, it is best to measure SAXS in SEC environment for reduced

degradation and with the addition benefit of separating protein from multimers and aggregates. It could also be possible to use SEC-SANS for a similar result.

3.7. Effect of lipids on the solution structure of mTSPO/amphiphile complex

We determined by SAXS the ratio of the most appropriate DMPC:DPC mixture so that the protein-free micelles are separated as far as possible in SEC from the mTSPO/DMPC:DPC complexes (Fig. S8A, Table S6). The size of DMPC:DPC micelles increased as a function of DMPC:DPC ratio, as shown by the smaller values of Q_{max} position, *i.e.* the Q-value at the maximum of the "bump" of the SAXS curves at large Q-values (Fig. S8, B-C). The more DMPC the micelles contain relative to DPC, the larger they are. However, the size of the micelles seems to reach a plateau, suggesting the saturation of lipids within mixed micelles. DMPC:DPC micelles with the reduced ratio of 1:2 were chosen because their size are significantly lower from that of the protein:belt complex, allowing greater peak separation by SEC.

SEC-SAXS of mTSPO in 0.05% DMPC:0.1% DPC (1:2) was measured at three concentrations (217, 328, and 433 µg of injected protein). The three concentration-normalized curves were nearly superimposed (weak attractive interactions are visible at $Q < 10^{-2}$ Å^{-1}). Therefore, over this range of concentration and Q, the structure factor $S(Q)$ is considered equal to 1 and the form factor remains constant (Fig. S5).

When comparing mTSPO/DMPC:DPC (1:2) complex (injection of 433 µg protein, Fig. S5) to mTSPO/SDS and mTSPO/DPC ones (the two latter being previously measured by SEC-SAXS[18]), the "bump" of the SEC-SAXS curve shifted to lower Q-values in presence of lipids (Fig. 6A, Table 2). It means the complex is significantly larger in DMPC:DPC compared to SDS, whereas it is smaller in DPC than in SDS[18]. This is confirmed by the Guinier analysis with R_g (46.9 Å) of mTSPO/belt complex that is greater in DMPC:DPC compared to SDS (37.0 Å) and DPC alone (31 Å) (Fig. 6A, insert, Table 2). This is consistent with the R_g in real space derived from the $P(r)$ curve (Table 2). The dimensionless Kratky representation shows that

mTSPO/DMPC:DPC complex presents a compact 3D structure in all amphiphilic conditions, as highlighted by the first maximum at $Q.R_g \approx \sqrt{3}$[39] (Fig. 6B).

The $P(r)$ pair distribution function exhibits negative and positive probabilities, which are interpreted as deviations to the mean SLD value: SLDs of mTSPO and of the amphiphilic head are both greater than the aqueous buffer SLD, whereas the SLD of the amphiphilic tail is lower (Table S2). The $P(r)$ is shifted to higher Q-values in DMPC:DPC compared to both SDS and DPC, and the maximum dimension (D_{max}) is significantly higher in DMPC:DPC (Fig. 6C, Table 2). Whereas the exchange from SDS to DPC reduces the complex and belt dimensions (Fig. 6, Table 2 and previously published data[18]), the addition of DMPC lipids induces a significant extension of the complex size. Assuming the protein remains in a monomeric state, as shown by SEC-MALLS analysis (Fig. 2 and previously published data[18]), and its size is comparable, or even reduced from SDS to DPC and DMPC:DPC due to refolding, the present results strongly suggest a more extended belt of DMPC:DPC compared to SDS and DPC. The D_{max} value is considered as the diameter of the whole complex, with a height roughly equal to the length of two amphiphile molecules, which might be comparable for DMPC:DPC to the thickness of a lipid bilayer (~40 Å).

Table 2. Structural results obtained from SEC-SAXS analysis (Fig. 6), in reciprocal (Guinier analysis) and real ($P(r)$ analysis) spaces, of mTSPO/belt complex in SDS, DPC, and DMPC:DPC (1:2) amphiphilic environments. The Q-value of the maximum of the "bump" of curves is precised (Q_{max}).

		mTSPO/SDS	**mTSPO/DPC**	**mTSPO/DMPC:DPC**
Reciprocal space	R_g (Å)	36.7 ± 0.1	30.5 ± 0.4	46.9 ± 0.9
	Q_{max} (Å^{-1})	0.18	0.20	0.12
Real space	R_g (Å)	35.80 ± 0.05	29.9 ± 0.1	46.9 ± 0.5

	D_{max} (Å)	115 ± 5	95 ± 2	142 ± 5

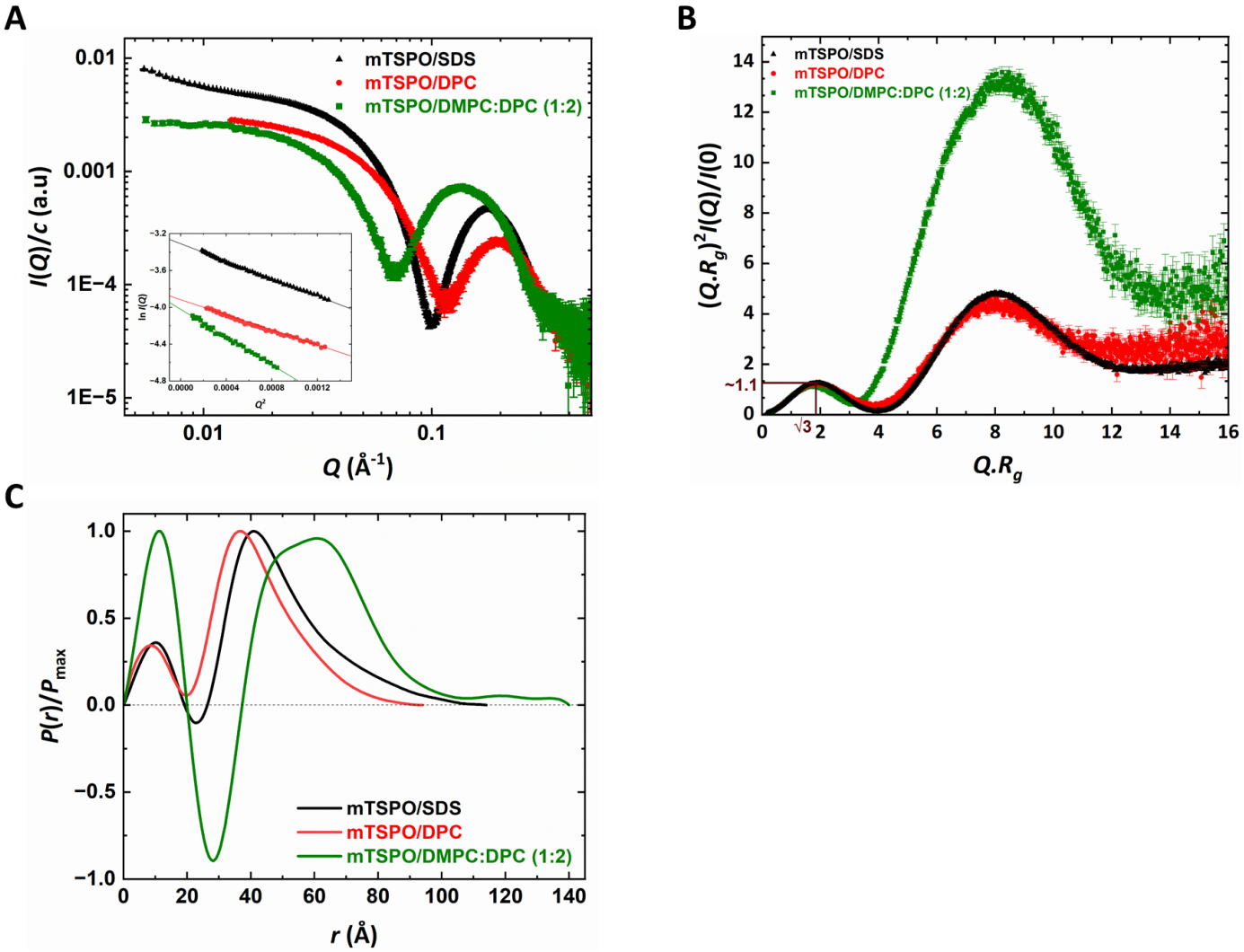

Figure 6. (***A***) SEC-SAXS curves of mTSPO in DMPC:DPC (ratio 1:2) compared to SDS and DPC environments (the two latter being previously[18]). *Inset:* corresponding Guinier plots. (***B***) Dimensionless Kratky representation and (***C***) pair-distance distribution function $P(r)$ (using GNOM[40], ATSAS) of the same data.

3.8. Effect of lipids on mTSPO affinity for PK11195 ligand

To our knowledge, this is the first-time that microscale thermophoresis (MST) is used to measure the affinity of mTSPO/belt complex for ligands. We used this innovative technique to determine the dissociation constants (K_d) of mTSPO for the (R)-PK11195 ligand. In comparison

to racemate, (R)-PK11195 is known to have higher affinity for mTSPO[41]. The K_d values indicate distinct binding characteristics depending on mTSPO amphiphilic belt: DPC-solubilized mTSPO exhibits an affinity of approximately 70 µM, while the DMPC:DPC (ratio 1:2)-solubilized mTSPO shows a significantly higher affinity with a K_d of 0.91 µM (Fig. 7, Eq. 5). These results demonstrate the major role of lipid environment in membrane protein–ligand recognition. In contrast, no interaction was observed for mTSPO solubilized in SDS detergent, in agreement with previous affinity ITC measurement[19]. This is correlated with the partially unfolded structure of mTSPO in this ionic surfactant[18]. However, upon exchanging SDS to the milder DPC detergent, mTSPO undergoes a refolded process and regains the ability to bind the ligand [8,22]. Even at rather low lipid:surfactant ratio (1:2), DMPC:DPC mixture significantly enhances mTSPO affinity for (R)-PK11195 ligand. This is quite surprising since the structural variations of mTSPO observed for this ratio are not yet very pronounced - significantly less than for the 2:1 ratio -, as shown by CD and Trp intrinsic fluorescence. (Figs. 3-4). This demonstrates that the presence of lipids, even at low concentration in mixed micelles, is very effective in inducing structural modifications of the mTSPO ligand binding regions, to allow greater accessibility of the ligand into the protein cavity. Previous results have demonstrated the ability of mTSPO to bind ligand at nanomolar affinity but while reconstituted in liposomes, *i.e.* in a pure lipidic environment[23]. Similar observations showed that the activity of ABC transporters is regained when reconstituted in lipidic environment compared to detergent micelles[42]. In addition, lipids are known to induce dynamic flexibility of the β-strands of the outer membrane protein OmpX, suggesting that the protein activity is more correlated with the protein flexibility, enhanced in a lipid environment, than its structural stability observed in detergents[43]. Mixed lipid: surfactant micelles could therefore provide both flexibility necessary for function and good stability for structure/function studies of membrane proteins in solution.

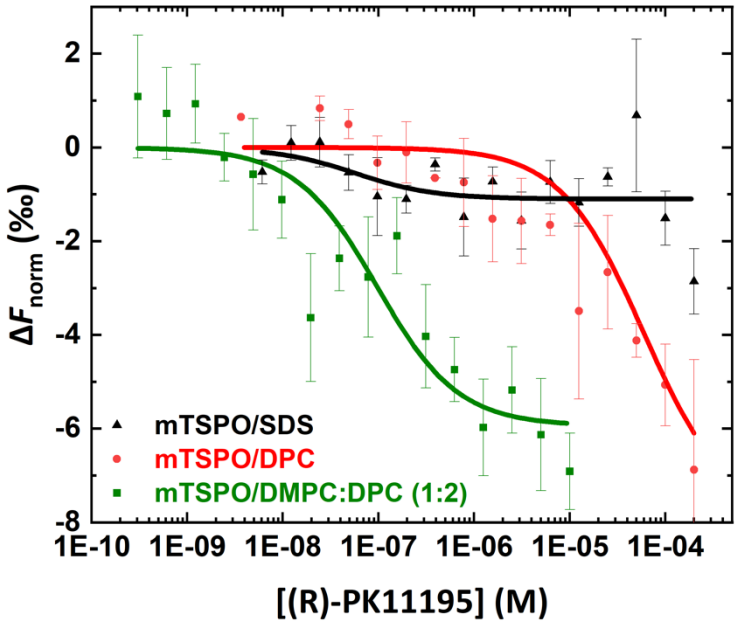

Figure 7. MST normalized measurements of mTSPO/SDS (black triangles), mTSPO/DPC (red circles), and mTSPO/DMPC:DPC (1:2 ratio, green squares) affinity for (R)-PK11195 ligand. The dissociation constant (K_d) was determined to be 70 µM in DPC and 0.91 µM in DMPC:DPC, whereas no binding was observed in SDS.

4. Conclusions

In conclusion, the present study reveals that replacement of detergent with a mixed lipid:detergent amphiphilic environment (DMPC:DPC) enhances the folding of SDS-purified recombinant apo-mTSPO compared to DPC alone. Such a more biomimetic environment stabilizes mTPSO by increasing the quantity of α-helices and their interactions, as well as the local structuring of Trp, while reducing protein aggregation. The amphiphilic belt of mTSPO is much more extensive in DMPC:DPC than in DPC. Importantly, this enhanced structuring induced by mixed lipid:surfactant micelles is associated with an increase in the affinity of mTSPO for the PK11195 ligand. The use of mixed lipid:surfactant micelles, such as DMPC:DPC, opens new possibilities for stabilizing and structuring membrane proteins to study their structure/function in solution in a more biomimetic amphiphilic environment.

ACKNOWLEDGMENTS

This project has received financial support from the CNRS through the MITI interdisciplinary program “Modélisation du vivant” (2021-2022). We thank the SANS-I (SINQ, PSI, Villigen, Switzerland) (proposal 20220915) and BM29 (ESRF, Grenoble, France) (“Paris rive gauche” BAG) beamlines for beamtime allocation. We thank also the French Infrastructure for Integrated Structural Biology (FRISBI) ANR-10-INSB-05 for MST experiments. We thank Dr Sana-Zineb Aimeur for the determination of the theoretical CD curve of mTSPO AlphaFold model using SESCA software and Sandrine Rosario of the “Plateforme de Biophysique Moléculaire” (PFBMI) of C2RT of Pasteur Institut (Paris, France) for DLS measurements and analysis.

REFERENCES

1. Lee Y, Park Y, Nam H, Lee JW, Yu SW. Translocator protein (TSPO): the new story of the old protein in neuroinflammation. *BMB Rep*. 2020;53(1):20-27. doi:10.5483/BMBRep.2020.53.1.273

2. Anholt RR, Pedersen PL, De Souza EB, Snyder SH. The peripheral-type benzodiazepine receptor. Localization to the mitochondrial outer membrane. *J Biol Chem*. 1986;261(2):576-583.

3. Braestrup C, Albrechtsen R, Squires RF. High densities of benzodiazepine receptors in human cortical areas. *Nature*. 1977;269(5630):702-704. doi:10.1038/269702a0

4. Papadopoulos V, Baraldi M, Guilarte TR, et al. Translocator protein (18kDa): new nomenclature for the peripheral-type benzodiazepine receptor based on its structure and molecular function. *Trends Pharmacol Sci*. 2006;27(8):402-409. doi:10.1016/j.tips.2006.06.005

5. Cheung G, Lin YC, Papadopoulos V. Translocator protein in the rise and fall of central nervous system neurons. *Front Cell Neurosci*. 2023;17:1210205. doi:10.3389/fncel.2023.1210205

6. Korkhov VM, Sachse C, Short JM, Tate CG. Three-dimensional structure of TspO by electron cryomicroscopy of helical crystals. *Struct Lond Engl 1993*. 2010;18(6):677-687. doi:10.1016/j.str.2010.03.001

7. Murail S, Robert JC, Coïc YM, et al. Secondary and tertiary structures of the transmembrane domains of the translocator protein TSPO determined by NMR.

Stabilization of the TSPO tertiary fold upon ligand binding. *Biochim Biophys Acta BBA - Biomembr*. 2008;1778(6):1375-1381. doi:10.1016/j.bbamem.2008.03.012

8. Jaremko Ł, Jaremko M, Giller K, Becker S, Zweckstetter M. Structure of the Mitochondrial Translocator Protein in Complex with a Diagnostic Ligand. *Science*. 2014;343(6177):1363-1366. doi:10.1126/science.1248725

9. Guo Y, Kalathur RC, Liu Q, et al. Protein structure. Structure and activity of tryptophan-rich TSPO proteins. *Science*. 2015;347(6221):551-555. doi:10.1126/science.aaa1534

10. Li F, Liu J, Zheng Y, Garavito RM, Ferguson-Miller S. Response to Comment on "Crystal structures of translocator protein (TSPO) and mutant mimic of a human polymorphism." *Science*. 2015;350(6260):519. doi:10.1126/science.aab2595

11. Liu J, Hiser C, Li F, Hall R, Garavito RM, Ferguson-Miller S. New TSPO Crystal Structures of Mutant and Heme-Bound Forms with Altered Flexibility, Ligand Binding, and Porphyrin Degradation Activity. *Biochemistry*. 2023;62(7):1262-1273. doi:10.1021/acs.biochem.2c00612

12. Li H, Papadopoulos V. Peripheral-type benzodiazepine receptor function in cholesterol transport. Identification of a putative cholesterol recognition/interaction amino acid sequence and consensus pattern. *Endocrinology*. 1998;139(12):4991-4997. doi:10.1210/endo.139.12.6390

13. Lacapere JJ, Duma L, Finet S, Kassiou M, Papadopoulos V. Insight into the Structural Features of TSPO: Implications for Drug Development. *Trends Pharmacol Sci*. 2020;41(2):110-122. doi:10.1016/j.tips.2019.11.005

14. Guo Y. Be Cautious with Crystal Structures of Membrane Proteins or Complexes Prepared in Detergents. *Crystals*. 2020;10(2):86. doi:10.3390/cryst10020086

15. Jaremko Ł, Jaremko M, Giller K, Becker S, Zweckstetter M. Conformational Flexibility in the Transmembrane Protein TSPO. *Chem Weinh Bergstr Ger*. 2015;21(46):16555-16563. doi:10.1002/chem.201502314

16. Duma L, Senicourt L, Rigaud B, Papadopoulos V, Lacapère JJ. Solid-state NMR study of structural heterogeneity of the apo WT mouse TSPO reconstituted in liposomes. *Biochimie*. 2023;205:73-85. doi:10.1016/j.biochi.2022.08.013

17. Zhang L, Hu K, Shao T, et al. Recent developments on PET radiotracers for TSPO and their applications in neuroimaging. *Acta Pharm Sin B*. 2021;11(2):373-393. doi:10.1016/j.apsb.2020.08.006

18. Combet S, Bonneté F, Finet S, et al. Effect of amphiphilic environment on the solution structure of mouse TSPO translocator protein. *Biochimie*. 2023;205:61-72. doi:10.1016/j.biochi.2022.11.014

19. Lacapere JJ, Iatmanen-Harbi S, Senicourt L, et al. Structural Studies of TSPO, a Mitochondrial Membrane Protein. In: *Membrane Proteins Production for Structural Analysis*. Springer: New York, NY, USA; Heidelberg/Berlin, Germany; Dordrecht, The Netherlands; London, UK,. ; 2014:393-421.

20. Li F, Liu J, Liu N, Kuhn LA, Garavito RM, Ferguson-Miller S. Translocator Protein 18 kDa (TSPO): An Old Protein with New Functions? *Biochemistry*. 2016;55(20):2821-2831. doi:10.1021/acs.biochem.6b00142

21. Iatmanen-Harbi S, Senicourt L, Papadopoulos V, Lequin O, Lacapere JJ. Characterization of the High-Affinity Drug Ligand Binding Site of Mouse Recombinant TSPO. *Int J Mol Sci*. 2019;20(6):1444. doi:10.3390/ijms20061444

22. Xia Y, Ledwitch K, Kuenze G, et al. A unified structural model of the mammalian translocator protein (TSPO). *J Biomol NMR*. 2019;73(6-7):347-364. doi:10.1007/s10858-019-00257-1

23. Lacapère JJ, Delavoie F, Li H, et al. Structural and Functional Study of Reconstituted Peripheral Benzodiazepine Receptor. *Biochem Biophys Res Commun*. 2001;284(2):536-541. doi:10.1006/bbrc.2001.4975

24. Horvath SE, Daum G. Lipids of mitochondria. *Prog Lipid Res*. 2013;52(4):590-614. doi:10.1016/j.plipres.2013.07.002

25. Le Maire M, Champeil P, Møller JV. Interaction of membrane proteins and lipids with solubilizing detergents. *Biochim Biophys Acta BBA - Biomembr*. 2000;1508(1-2):86-111. doi:10.1016/S0304-4157(00)00010-1

26. Koynova R, Caffrey M. Phases and phase transitions of the phosphatidylcholines. *Biochim Biophys Acta BBA - Rev Biomembr*. 1998;1376(1):91-145. doi:10.1016/S0304-4157(98)00006-9

27. Booth PJ, Flitsch SL, Stern LJ, Greenhalgh DA, Kim PS, Khorana HG. Intermediates in the folding of the membrane protein bacteriorhodopsin. *Nat Struct Mol Biol*. 1995;2(2):139-143. doi:10.1038/nsb0295-139

28. Gourdon P, Andersen JL, Hein KL, et al. HiLiDe—Systematic Approach to Membrane Protein Crystallization in Lipid and Detergent. *Cryst Growth Des*. 2011;11(6):2098-2106. doi:10.1021/cg101360d

29. Senicourt L, Iatmanen-Harbi S, Hattab C, Ostuni MA, Giraud MF, Lacapere JJ. Recombinant Overexpression of Mammalian TSPO Isoforms 1 and 2. *Methods Mol Biol Clifton NJ*. 2017;1635:1-25. doi:10.1007/978-1-4939-7151-0_1

30. Gimpl K, Klement J, Keller S. Characterising protein/detergent complexes by triple-detection size-exclusion chromatography. *Biol Proced Online*. 2016;18(1):4. doi:10.1186/s12575-015-0031-9

31. Micsonai A, Wien F, Kernya L, et al. Accurate secondary structure prediction and fold recognition for circular dichroism spectroscopy. *Proc Natl Acad Sci U S A*. 2015;112(24):E3095-3103. doi:10.1073/pnas.1500851112

32. Hammouda B. SANS from homogeneous polymer mixtures: A unified overview. In: *Polymer Characteristics*. Vol 106. Advances in Polymer Science. Springer-Verlag; 1993:87-133. doi:10.1007/BFb0025862

33. Mildner DFR, Hall PL. Small-angle scattering from porous solids with fractal geometry. *J Phys Appl Phys*. 1986;19(8):1535-1545. doi:10.1088/0022-3727/19/8/021

34. Tully MD, Kieffer J, Brennich ME, et al. BioSAXS at European Synchrotron Radiation Facility – Extremely Brilliant Source: BM29 with an upgraded source, detector, robot, sample environment, data collection and analysis software. *J Synchrotron Radiat*. 2023;30(1):258-266. doi:10.1107/S1600577522011286

35. Tully MD, Tarbouriech N, Rambo RP, Hutin S. Analysis of SEC-SAXS data via EFA deconvolution and Scatter. *J Vis Exp*. 2021;(167):61578. doi:10.3791/61578

36. Hopkins JB, Gillilan RE, Skou S. BioXTAS RAW: improvements to a free open-source program for small-angle X-ray scattering data reduction and analysis. *J Appl Crystallogr*. 2017;50(Pt 5):1545-1553. doi:10.1107/S1600576717011438

37. Nagy G, Igaev M, Jones NC, Hoffmann SV, Grubmüller H. SESCA: Predicting Circular Dichroism Spectra from Protein Molecular Structures. *J Chem Theory Comput*. 2019;15(9):5087-5102. doi:10.1021/acs.jctc.9b00203

38. Hedger G, Sansom MSP. Lipid interaction sites on channels, transporters and receptors: Recent insights from molecular dynamics simulations. *Biochim Biophys Acta BBA - Biomembr*. 2016;1858(10):2390-2400. doi:10.1016/j.bbamem.2016.02.037

39. Burger VM, Arenas DJ, Stultz CM. A Structure-free Method for Quantifying Conformational Flexibility in proteins. *Sci Rep*. 2016;6(1):29040. doi:10.1038/srep29040

40. Manalastas-Cantos K, Konarev PV, Hajizadeh NR, et al. ATSAS 3.0: expanded functionality and new tools for small-angle scattering data analysis. *J Appl Crystallogr*. 2021;54(Pt 1):343-355. doi:10.1107/S1600576720013412

41. Shah F, Hume SP, Pike VW, Ashworth S, McDermott J. Synthesis of the enantiomers of [N-methyl-11C]PK 11195 and comparison of their behaviours as radioligands for PK binding sites in rats. *Nucl Med Biol*. 1994;21(4):573-581. doi:10.1016/0969-8051(94)90022-1

42. Neumann J, Rose-Sperling D, Hellmich UA. Diverse relations between ABC transporters and lipids: An overview. *Biochim Biophys Acta BBA - Biomembr*. 2017;1859(4):605-618. doi:10.1016/j.bbamem.2016.09.023

43. Frey L, Lakomek N, Riek R, Bibow S. Micelles, Bicelles, and Nanodiscs: Comparing the Impact of Membrane Mimetics on Membrane Protein Backbone Dynamics. *Angew Chem Int Ed*. 2017;56(1):380-383. doi:10.1002/anie.201608246